

The Orbits of the γ -ray Binaries LS I +61 303 and LS 5039

Christina Aragona, M. Virginia McSwain

Department of Physics, Lehigh University, 16 Memorial Drive East, Bethlehem, PA 18015
 cha206@lehigh.edu, mcswain@lehigh.edu

Erika D. Grundstrom

Physics and Astronomy Department, Vanderbilt University, 6301 Stevens Center, Nashville, TN 37235
 erika.grundstrom@vanderbilt.edu

Amber N. Marsh, Rachael M. Roettenbacher, Katelyn M. Hessler

Department of Physics, Lehigh University, 16 Memorial Drive East, Bethlehem, PA 18015
 anm506@lehigh.edu, rmr207@lehigh.edu, kmh410@lehigh.edu

Tabetha S. Boyajian

Center for High Angular Resolution Astronomy and Department of Physics and Astronomy, Georgia State University, Atlanta, GA
 boyajian@chara.gsu.edu

Paul S. Ray

Space Science Division, Naval Research Laboratory, Washington DC, 20375
 paul.ray@nrl.navy.mil

ABSTRACT

LS I +61 303 and LS 5039 are two of only a handful of known high mass X-ray binaries (HMXBs) that exhibit very high energy emission in the MeV-TeV range, and these “ γ -ray binaries” are of renewed interest due to the recent launch of the *Fermi Gamma-ray Space Telescope*. Here we present new radial velocities of both systems based on recent red and blue optical spectra. Both systems have somewhat discrepant orbital solutions available in the literature, and our new measurements result in improved orbital elements and resolve the disagreements. The improved geometry of each orbit will aid in studies of the high energy emission region near each source.

Subject headings: binaries: spectroscopic – stars: individual(LS 5039, LS I +61 303)

1. Introduction

LS I +61 303 is a Be/X-ray binary with spectral type B0 Ve, a 26.5 day orbital period, and highly eccentric orbit (Grundstrom et al. 2007a; Casares et al. 2005a). High energy emission from LS I +61 303 was first detected 30 years ago

(as γ -ray source CG 135+1) by the Cosmic Ray Satellite B (Hermsen et al. 1977). Shortly thereafter, NASA’s Einstein Observatory and ground based radio observations suggested that the system was no ordinary HMXB (Gregory & Taylor 1978; Bignami & Hermsen 1983). While the system has a relatively low X-ray luminosity for a

HMXB, LS I +61 303 is one of the 20 brightest γ -ray sources known. The Be disk interacts with the compact companion, either a neutron star or black hole, producing orbital phase modulated emission across the electromagnetic spectrum: TeV (Albert et al. 2006, 2008), X-ray (Paredes et al. 1997; Leahy 2001), optical $H\alpha$ (Grundstrom et al. 2007a), and radio flux (Gregory & Taylor 1978; Taylor et al. 1992).

LS 5039 is a HMXB that consists of a massive, main sequence primary (ON6.5 V((f)) spectral type; McSwain et al. 2004) and a compact companion in a tightly bound, eccentric orbit (Casares et al. 2005b). Optical and UV spectra of the system reveal nitrogen enrichment and carbon depletion at the surface of the O star, a sign of prior mass transfer that inverted the binary mass ratio before the supernova occurred (McSwain et al. 2004). The binary remained bound and was ejected from the Galactic plane within the past 1.1 Myr in an asymmetric supernova explosion that imparted a runaway velocity of about 150 km s^{-1} to the system (Ribó et al. 2002; McSwain et al. 2004). As a HMXB, LS 5039 is quite inconspicuous with a relatively constant, low X-ray flux and hard spectrum; it does not experience dramatic X-ray flares or state changes that are seen in most other HMXBs. However, it is an unusually bright radio source for a HMXB (Ribó et al. 1999). The system distinguished itself when it was first noted as a probable γ -ray source by Paredes et al. (2000) since it is the only simultaneous X-ray and radio emitter inside the 95% confidence contour of the EGRET source 3EG J1824–1514. Its bright and hard γ -ray spectrum suggested that it might be observable by ground-based atmospheric Cherenkov telescope arrays, and indeed it was detected with energies $> 0.1 \text{ TeV}$ by the HESS array (Aharonian et al. 2005a). The identification of the γ -ray source with the optical star LS 5039 was strengthened by the γ -ray variability over the 4 day orbital period (Aharonian 2006). The X-ray flux is also modulated with the orbital period (Bosch-Ramon et al. 2005, 2007; Takahashi et al. 2008).

LS I +61 303 and LS 5039 are two of only five known HMXBs that exhibit very high energy emission in the MeV-TeV range (“ γ -ray binaries”); the others are PSR B1259–63 (Cominsky et al. 1994; Aharonian et al. 2005b), Cygnus X-1 (Albert et

al. 2007), and the recently proposed candidate HESS J0632+057 (Hinton et al. 2009). The recent launch of the *Fermi Gamma-ray Space Telescope* heralds a new era in the understanding of very high energy emission of these sources, and our group is currently involved in multiwavelength observing campaigns for both systems. In an effort to support these programs, we present here new optical spectroscopy and radial velocity measurements of LS I +61 303 in §2 and LS 5039 in §3. We discuss the results and the implications of the new orbits in §4.

2. Observations and Radial Velocity Measurements of LS I +61 303

We obtained 83 spectra of LS I +61 303 at the KPNO coude feed telescope over 35 consecutive nights during 2008 October and November. We used grating B in second order with the OG550 order-sorting filter and the F3KB detector. The spectra were wavelength calibrated using ThAr comparison lamp spectra taken throughout each night. This instrumental configuration resulted in a wavelength range of 6400–7050 Å with a resolving power $R = \lambda/\Delta\lambda$ ranging from 11400–12500 across the chip.

We generally obtained 2–3 spectra of 30 minutes duration each night. The images were zero corrected, flat fielded, and wavelength calibrated using standard procedures in IRAF¹. The spectra were interpolated onto a log wavelength scale using a common heliocentric wavelength grid, and they were rectified to a unit continuum using line-free regions.

Our red spectra of LS I +61 303 include only two prominent stellar features, $H\alpha$ and He I $\lambda 6678$, shown in Figure 1. The $H\alpha$ line is dominated by double-peaked emission from the circumstellar disk of the Be star. While the absorption trough does follow the orbital motion of the star, we did not use this line to measure the spectroscopic orbit since its radial velocity, V_r , measurements may be strongly affected by changes in the disk structure. Weak emission is also present in the blue and red wings of the He I $\lambda 6678$ line, but it is less affected

¹IRAF is distributed by the National Optical Astronomy Observatory, which is operated by the Association of Universities for Research in Astronomy, Inc., under cooperative agreement with the National Sciences Foundation

by temporal changes in the disk. Therefore we measured radial velocities of LS I +61 303 using only this line.

We formed a reference spectrum of LS I +61 303 using the mean of all available spectra (without shifting to their rest velocity to avoid any prior assumptions about the orbit), and we measured the V_r of this mean spectrum using a parabolic fit of the He I $\lambda 6678$ line core. Since we were concerned that the emission in the line wings (rather than the photospheric absorption component) might affect the relative velocities, we excised the emission on the blue and red wings of the reference spectrum to a unit continuum. We then performed a cross correlation between each spectrum and this reference spectrum over the He I $\lambda 6678$ line region to obtain the relative V_r , which we added to the V_r of the reference spectrum to obtain the absolute V_r . We also measured the cross correlation velocity shift of the interstellar line at 6613 \AA , ΔV_{ISM} , using the same method to monitor the stability of our measurements. After removing measurements with $|V_{\text{ISM}}| > 5 \text{ km s}^{-1}$ and spectra in which the He I $\lambda 6678$ line profile was strongly affected by cosmic rays, we present a total of 75 V_r measurements in Table 1.

The orbital period of LS I +61 303 is well known from radio flux observations (Gregory 2002), so we adopted the period $26.4960 \pm 0.0028 \text{ d}$ from that work. Many recent papers also use an arbitrary orbital phase, $\phi(\text{TG})$, defined to be zero at HJD $2,443,366.775$ (Taylor & Gregory 1982), which we adopt as well. Our V_r agree well with Casares et al. (2005a), but measurements from Grundstrom et al. (2007a) are systematically lower by 8.8 km s^{-1} (based on the difference in the center of mass velocity, γ , using each data set separately). This difference is likely due to a small difference in the rest wavelength of that line; we used 6678.15 \AA as given by the NIST Atomic Spectra Database (Ralchenko et al. 2008). Therefore we offset their V_r by this amount to determine the orbital elements of LS I +61 303, and we excluded their points with discrepant V_{ISM} values as well. Using this edited set of V_r from Casares et al. (2005a), Grundstrom et al. (2007a), and this work, we determined the orbital elements using the non-linear, least-squares fitting program of Morbey & Brosterhus (1974). There are several points with large scatter and a systematic trend

in the V_r curve (discussed in §4), so we assigned zero weight to points with $|O - C| > 2\sigma$ and refit the orbit for the final orbital solution.

The resulting time of periastron, T_0 , eccentricity, e , angle of the line of nodes, ω , velocity semi-amplitude, K_1 , center of mass velocity, γ , mass function, $f(m)$, projected separation, $a_1 \sin i$, and the standard deviation of the fit, σ , are listed in column 2 of Table 2. The final V_r curve is shown in Figure 2, and the orbital phases (relative to Taylor & Gregory 1982) and observed minus corrected errors ($O - C$) are included in Table 1. With our new orbital fit, the orbital phase of periastron is $\phi(\text{TG}) = 0.275$.

The geometry of the orbit is illustrated in Figure 3, assuming a Be star mass of $12.5M_\odot$ (Casares et al. 2005a) with either a neutron star ($1.4M_\odot$) or a black hole ($4M_\odot$) companion. Except for γ , each orbital element agrees very well with the values found by Grundstrom et al. (2007a). Because our spectra of LS I +61 303 were obtained over 35 consecutive nights, our V_r measurements provide excellent coverage of the orbit with no large gaps in orbital phase, and the errors in our fit are slightly lower than those of Grundstrom et al. (2007a) and significantly lower than those of Casares et al. (2005a). We also emphasize that our final orbital solution relies upon the fixed P from Gregory (2002), but we found very similar values for each orbital element when we allowed P to vary. We found $P = 26.4982 \pm .0076 \text{ d}$ using the fitting program of Morbey & Brosterhus (1974) with the combined V_r data, which is not an improvement over Gregory (2002).

3. Observations and Radial Velocity Measurements of LS 5039

Spectra of LS 5039 were taken at the CTIO 1.5m telescope between 2007 August and 2008 April in service mode. We used grating 47 in the second order, a 200 micron slit, the BG39 filter, and the Loral 1K CCD detector. Spectra were wavelength calibrated using HeAr comparison lamp spectra generally taken before and after each exposure. The observed wavelength region was therefore about $4050\text{--}4700 \text{ \AA}$, with $2500 < R < 3150$ across the chip.

For each night that we had service time available in fall 2007, we obtained 4-6 spectra, each

with an exposure time of 30 minutes. During the spring of 2008, we obtained 2 spectra each night of observations, each of 22 minutes duration. Thus we obtained a total of 98 blue spectra of LS 5039. The images were zero corrected, flat fielded, and wavelength calibrated onto a log wavelength scale using standard procedures in IRAF, and all spectra were interpolated onto a common heliocentric wavelength grid. The spectra were rectified to a unit continuum using line-free regions.

Since the signal-to-noise (S/N) ratio was somewhat low, we chose to coadd pairs of consecutive spectra from each night. The total elapsed time during two consecutive observations is only one hour, about 1% of the orbital period, so coadding the spectra does not significantly affect the measured V_r . On two nights we collected an odd number of spectra, and in these cases the last spectrum of each set was examined individually. Therefore, we had 50 new spectra from which to obtain V_r measurements and improve the orbital elements.

The spectra from August 29, 2007 were taken near the time of inferior conjunction and thus showed the least variation in V_r , so we chose to average these six spectra to produce a reference spectrum. This reference spectrum is plotted in Figure 4. Five lines were examined in each spectrum: H γ , H δ , He II $\lambda\lambda$ 4200, 4542, and He I λ 4471. The spectra also recorded the strong He II λ 4686 line, but a bad column on the chip interfered with measuring reliable V_r from this line. We performed a cross correlation between each spectrum and the reference spectrum to obtain its relative V_r , and then we used the mean V_r from a parabolic fit of the line cores in the reference spectrum to find its absolute V_r .

The period of the system was obtained using the discrete Fourier transform and CLEAN deconvolution program of Roberts, Lehár, & Dreher (1987) (written in IDL² by A. W. Fullerton). The V_r from our observations were combined with the mean values from all lines measured by McSwain et al. (2001), McSwain et al. (2004), and Casares et al. (2005b). The V_r measurements of Casares et al. (2005b) indicate a value of γ that is systematically higher than our data sets by 7.0 km s^{-1} , so we subtracted this value from their measurements. No significant difference was found between the V_r

data presented here and past measurements obtained by our group. We used all of the available V_r with the CLEAN algorithm, which found a strong peak at $P = 3.9060263 \text{ d}$ (which was improved slightly with the later orbital fit), nearly identical to the period found by Casares et al. (2005b). Our group has previously found $P = 4.1 \text{ d}$ (McSwain et al. 2001) and $P = 4.4 \text{ d}$ (McSwain et al. 2004) for LS 5039, due to the very high scatter in its V_r curve, which has led to considerable confusion about the correct orbital period of this system. We note that our period search also resulted in $P = 3.906 \text{ d}$ when we excluded the data of Casares et al. (2005b), so we have added confidence that this is indeed the correct period for LS 5039. We also investigated other weak frequency signals found by CLEAN, but these periods did not produce a realistic V_r curve.

We determined the remaining orbital elements with the non-linear, least-squares fitting program of Morbey & Brosterhus (1974) to solve for the orbital elements. With each point assigned equal weight, the resulting orbital elements are displayed in column 3 of Table 2. Our times of observations, orbital phases, V_r measurements, and $(O - C)$ errors are listed in Table 1. The standard deviation of V_r from the mean of all five lines is comparable to the $(O - C)$ error. Figure 5 illustrates the radial velocity curve using all available V_r measurements.

For our new orbital fit of LS 5039, the geometry is illustrated in Figure 6. In this figure, we show the relative orbit of the optical star with $23M_\odot$ (Casares et al. 2005b) and a compact companion. Casares et al. (2005b) have proposed a $3.7M_\odot$ black hole in the system, although Dubus (2006) favors a neutron star ($1.4M_\odot$) companion. Our orbital solution is not very different from the fit found by Casares et al. (2005b) using all available H, He I, and He II lines. However, they adopt a final solution found using only the He II lines, which results in a slightly higher e , γ , and K_1 than our result. Their argument that wind emission in the O star may affect the line species differently, whereas the He II line is formed in the photosphere and is less contaminated by the wind, is very reasonable. However, we did not observe systematic line-to-line differences in our spectra, and the scatter for all lines is equally large. Therefore we favor using the mean of all available lines for the orbital solution of LS 5039.

²IDL is a registered trademark of Research Systems, Inc.

4. Discussion

Both LS I +61 303 and LS 5039 have previously published orbital solutions in the literature with large disagreements in the orbital elements (McSwain et al. 2001, 2004; Casares et al. 2005a,b; Grundstrom et al. 2007a). The need for an improved system geometry, especially in LS I +61 303, was highlighted recently by Sierpowska-Bartosik & Torres (2008) because the stellar separation and wind density play a significant role in the location of the γ -ray emission region (Dubus 2006) and opacities in a pulsar wind zone model. In fact, they found that a putative wind shock region in LS I +61 303 could lie unphysically close to the optical star using the orbital solution of Casares et al. (2005a) along with several assumptions about the stellar and pulsar wind strengths. Our new solution for LS I +61 303 results in a larger separation distance at periastron, so the stand-off distance of the shock region will be correspondingly farther from the star for the same wind parameters. Since the γ -ray production and its opacities are very sensitive to the orbital geometry, our spectroscopic orbital solutions of LS I +61 303 and LS 5039 may be further improved and the system inclinations constrained using their MeV-TeV light curves.

We note that the radial velocity curves of both LS I +61 303 and LS 5039 reveal a large number of spurious V_r points near apastron. In the case of LS I +61 303, Figure 2 indicates a secondary maximum in the V_r curve near $\phi \sim 0.8$ that appears both in our observations and those of Grundstrom et al. (2007a). To examine this behavior more carefully, we show in Figure 7 the He I $\lambda 6678$ line profiles and a gray-scale image of this line over our 35 consecutive nights of observation. Some glitches that do not affect the absorption line profile have been removed for clarity. Note that neither the line profiles nor gray-scale plots are folded by orbital phase, but rather they reveal true chronological variations in the line profile behavior as a function of HJD and the corresponding orbital phase. Our spectra between $0.6 \lesssim \phi(\text{TG}) \lesssim 0.7$ reveal a slight increase in both the red (R) and violet (V) emission peaks, followed by a decline in emission between $0.7 \lesssim \phi(\text{TG}) \lesssim 0.9$. The effect is much more pronounced in the $H\alpha$ line profile and was also noted by Grundstrom et al. (2007a).

Thus the V and R variations appear to be related to cyclic orbital variations rather than an isolated event. Although one spectrum does contain a sharp glitch in the line core (not included in our V_r measurements), the secondary V_r increase near $\phi(\text{TG}) \sim 0.8$ is due to the decrease in emission strength and the corresponding broadening of the absorption line profile.

In LS 5039, most of the spurious points in the V_r curve occur between $0.4 \lesssim \phi \lesssim 0.6$, and they have been observed by other authors as well (McSwain et al. 2001, 2004; Casares et al. 2005b). In fact, the frequent deviations in V_r are the main source of confusion in the orbital elements published by these authors. Our low spectral resolution does not permit a detailed analysis of the line behavior at this time, but higher resolution spectra may provide evidence of systematic line profile changes in the system.

We gratefully acknowledge the anonymous referee for helpful comments about this manuscript as well as Jorge Casares for sharing his radial velocity measurements of LS 5039. We also thank Di Harmer and the staff at KPNO, as well as Fred Walter and the SMARTS service observers, for their hard work to schedule and support these observations. This work is supported by NASA DPR numbers NNX08AV70G, NNX08AX79G, and NNG08E1671 and an institutional grant from Lehigh University.

Facilities: CTIO:1.5m, KPNO:CFT

REFERENCES

- Aharonian, F., et al. 2005a, *Science*, 309, 746
- Aharonian, F., et al. 2005b, *A&A*, 442, 1
- Aharonian, F., et al. 2006, *A&A*, 460, 743
- Albert, J., et al. 2006, *Science*, 312, 1771
- Albert, J., et al. 2007, *ApJ*, 665, L51
- Albert, J., et al. 2008, arXiv0806.1865
- Bignami, G. F., & Hermsen, W. 1983, *ARA&A*, 21, 67
- Bosch-Ramon, V., Paredes, J. M., Ribó, M., Miller, J. M., Reig, P., & Martí, J. 2005, *ApJ*, 628, 388

- Bosch-Ramon, V., et al. 2007, *A&A*, 473, 545
- Casares, J., Ribas, I., Paredes, J. M., Martí, J., & Allende Prieto, C. 2005a, *MNRAS*, 360, 1105
- Casares, J., Ribó, M., Ribas, I., Paredes, J. M., Martí, J., & Herrero, A. 2005b, *MNRAS*, 364, 899
- Cominsky, L., Roberts, M., & Johnston, S. 1994, *ApJ*, 427, 978
- Cordes, J. M., & Lazio, T. J. W. 2002, arXiv0207156
- de Naurois, M. 2007, *Ap&SS*, 309, 277
- Dubus, G. 2006, *A&A*, 456, 801
- Gregory, P. C. 2002, *ApJ*, 575, 427
- Gregory, P. C., & Taylor, A. R. 1978, *Nature*, 272, 704
- Grundstrom, E. D., Caballero-Nieves, S. M., Gies, D. R., Huang, W., McSwain, M. V., Rafter, S. E., Riddle, R. L., Williams, S. J., Wingert, D. W. 2007a, *ApJ*, 656, 437
- Grundstrom, E. D., Gies, D. R., Hillwig, T. C., McSwain, M. V., Smith, N., Gehrz, R. D., Stahl, O., & Kaufer, A. 2007b, *ApJ*, 667, 505
- Hermesen, W., et al. 1977, *Nature*, 269, 494
- Hinton, J. A., et al. 2009, *ApJ*, 690, L101
- Leahy, D. A. 2001, *A&A*, 380, 516
- McSwain, M. V., Gies, D. R., Riddle, R. L., Wang, Z., & Winger, D. W. 2001, *ApJ*, 558, L43
- McSwain, M. V., Gies, D. R., Huang, W., Wiita, P. J., Wingert, D. W., & Kaper, L. 2004, *ApJ*, 600, 927
- Morbey, C. L., & Brosterhus, E. B. 1974, *PASP*, 86, 455
- Okazaki, A. T., Bate, M. R., Ogilvie, G. I., & Pringle, J. E. 2002, *MNRAS*, 337, 967
- Paredes, J. M., Martí, J., Peracaula, M., & Ribó, M. 1997, *A&A*, 320, L25
- Paredes, J. M., Martí, J., Ribó, M., & Massi, M. 2000, *Science*, 288, 2340
- Ribó, M., Paredes, J. M., & Martí, J. 1999, *New Astronomy Reviews*, 43, 545
- Ralchenko, Yu., Kramida, A. E., Reader, J., & NIST ASD Team 2008, NIST Atomic Spectra Database (version 3.1.5), [Online]. Available: <http://physics.nist.gov/asd3> [2009, February 15]. National Institute of Standards and Technology, Gaithersburg, MD
- Ribó, M., Paredes, J. M., Romero, G. E., Benaglia, P., Martí, J., Fors, O., & García-Sánchez, J. 2002, *A&A*, 384, 954
- Roberts, D. H., Lehár, J., & Dreher, J. W. 1987, *AJ*, 93, 968
- Sierpowska-Bartosik, A., & Torres, D. F. 2008, arXiv0811.2466v1
- Takahashi, T., et al. 2008, arXiv0812.3358
- Taylor, A. R., & Gregory, P. C. 1982, *ApJ*, 255, 210
- Taylor, A. R., Kenny, H. T., Spencer, R. E., & Tzioumis, A. 1992, *ApJ*, 395, 268

This 2-column preprint was prepared with the AAS L^AT_EX macros v5.2.

TABLE 1
RADIAL VELOCITY MEASUREMENTS

Star	HJD (-2,450,000)	Orbital Phase	V_r (km s ⁻¹)	($O - C$) (km s ⁻¹)	ΔV_{ISM} (km s ⁻¹)
LS I +61°303	4757.6644	0.910	-54.7	-11.1	3.92
LS I +61°303	4758.6607	0.947	-62.0	-20.1	-2.44
LS I +61°303	4758.6827	0.948	-61.3	-19.4	-0.42
LS I +61°303	4759.6877	0.986	-53.9	-14.0	-0.59
LS I +61°303	4759.7088	0.987	-52.7	-12.8	3.97
LS I +61°303	4760.6803	0.024	-42.8	-5.1	-1.21
LS I +61°303	4760.7014	0.024	-49.5	-11.8	-0.60
LS I +61°303	4761.7508	0.064	-41.1	-6.3	0.21
LS I +61°303	4761.7719	0.065	-40.1	-5.3	-1.38
LS I +61°303	4762.6955	0.100	-23.3	8.4	1.87
LS I +61°303	4762.7166	0.101	-21.9	9.8	0.74
LS I +61°303	4763.7018	0.138	-32.3	-4.7	2.48
LS I +61°303	4763.7229	0.139	-18.7	8.7	1.13
LS I +61°303	4764.6373	0.173	-18.4	4.4	2.84
LS I +61°303	4764.6583	0.174	-18.5	4.2	0.74
LS I +61°303	4765.0282	0.188	-10.2	10.4	1.82
LS I +61°303	4765.6837	0.213	-18.5	-1.8	2.87
LS I +61°303	4765.9010	0.221	-7.1	8.5	-0.42
LS I +61°303	4765.9221	0.222	-16.0	-0.5	-2.31
LS I +61°303	4766.7893	0.254	-15.4	-1.1	0.14
LS I +61°303	4766.8574	0.257	-15.8	-1.2	-4.19
LS I +61°303	4766.9291	0.260	-17.8	-2.8	-2.97
LS I +61°303	4767.7007	0.289	-25.4	-1.6	0.01
LS I +61°303	4767.7805	0.292	-26.0	-1.0	-2.20
LS I +61°303	4767.8459	0.294	-32.8	-6.8	-0.05
LS I +61°303	4768.7456	0.328	-48.9	-10.3	-1.69
LS I +61°303	4768.8149	0.331	-54.5	-15.2	0.32
LS I +61°303	4768.8841	0.333	-59.0	-18.9	-1.01
LS I +61°303	4769.7368	0.365	-35.6	11.0	-2.74
LS I +61°303	4769.7970	0.368	-37.8	9.2	-0.60
LS I +61°303	4769.8738	0.371	-46.4	1.0	-1.05
LS I +61°303	4770.7309	0.403	-59.8	-9.3	-0.65
LS I +61°303	4770.7911	0.405	-72.0	-21.4	2.43
LS I +61°303	4770.8624	0.408	-47.4	3.3	-0.92
LS I +61°303	4771.8542	0.445	-46.1	6.2	0.64
LS I +61°303	4771.8753	0.446	-45.9	6.5	-0.43
LS I +61°303	4773.7536	0.517	-55.7	-2.7	-1.52
LS I +61°303	4773.7752	0.518	-48.8	4.2	-0.01
LS I +61°303	4774.9024	0.560	-40.5	12.2	-2.28
LS I +61°303	4775.7528	0.593	-56.2	-3.9	-0.77

TABLE 1—*Continued*

Star	HJD (−2,450,000)	Orbital Phase	V_r (km s ^{−1})	($O - C$) (km s ^{−1})	ΔV_{ISM} (km s ^{−1})
LS I +61°303	4776.7648	0.631	−67.9	−16.2	2.28
LS I +61°303	4776.7862	0.632	−62.6	−11.0	−0.37
LS I +61°303	4777.7764	0.669	−54.7	−3.8	0.17
LS I +61°303	4777.8919	0.673	−58.2	−7.4	0.99
LS I +61°303	4778.7466	0.706	−57.2	−7.1	−1.14
LS I +61°303	4778.7677	0.706	−62.9	−12.8	1.41
LS I +61°303	4779.6636	0.740	−40.1	9.1	0.96
LS I +61°303	4779.6851	0.741	−34.7	14.5	1.70
LS I +61°303	4781.7344	0.818	−18.8	28.2	0.87
LS I +61°303	4782.6531	0.853	−23.4	22.5	1.16
LS I +61°303	4782.8258	0.859	−38.8	6.8	−1.88
LS I +61°303	4782.8470	0.860	−31.4	14.1	−0.54
LS I +61°303	4784.6952	0.930	−48.7	−5.9	−2.14
LS I +61°303	4784.7163	0.931	−52.8	−10.1	−0.96
LS I +61°303	4784.7536	0.932	−43.4	−0.7	1.90
LS I +61°303	4784.7747	0.933	−47.3	−4.7	−2.93
LS I +61°303	4785.8022	0.972	−47.0	−6.2	−1.47
LS I +61°303	4785.8233	0.973	−45.5	−4.9	−3.56
LS I +61°303	4786.7401	0.007	−29.8	9.0	2.78
LS I +61°303	4786.7612	0.008	−33.7	5.0	−0.71
LS I +61°303	4787.6918	0.043	−29.0	7.4	0.50
LS I +61°303	4787.7129	0.044	−32.1	4.2	2.14
LS I +61°303	4787.7340	0.045	−32.7	3.6	−0.47
LS I +61°303	4787.7551	0.046	−50.2	−13.9	1.13
LS I +61°303	4787.7762	0.046	−31.6	4.6	−1.42
LS I +61°303	4788.8069	0.085	−31.9	1.2	−3.15
LS I +61°303	4788.8280	0.086	−32.2	0.8	−3.10
LS I +61°303	4789.6443	0.117	−25.2	4.8	2.02
LS I +61°303	4789.6654	0.118	−23.7	6.1	1.22
LS I +61°303	4790.7113	0.157	−26.8	−1.7	−1.50
LS I +61°303	4790.7324	0.158	−23.1	1.9	0.90
LS I +61°303	4790.7536	0.159	−17.9	6.9	−1.35
LS I +61°303	4790.7747	0.159	−25.0	−0.3	−1.89
LS I +61°303	4791.7059	0.195	−8.8	10.7	−1.40
LS I +61°303	4791.7270	0.195	−25.4	−6.0	−1.92
LS 5039	4315.5746	0.351	21.9	4.1	...
LS 5039	4315.6176	0.362	20.3	2.9	...
LS 5039	4315.6607	0.373	15.1	−1.9	...
LS 5039	4316.6470	0.626	3.1	−0.3	...
LS 5039	4316.6900	0.637	−0.5	−3.1	...

TABLE 1—*Continued*

Star	HJD (−2,450,000)	Orbital Phase	V_r (km s ^{−1})	($O - C$) (km s ^{−1})	ΔV_{ISM} (km s ^{−1})
LS 5039	4330.4876	0.169	22.0	3.9	...
LS 5039	4330.5296	0.180	28.4	9.8	...
LS 5039	4330.5716	0.190	20.9	1.8	...
LS 5039	4333.6362	0.975	−17.4	−1.8	...
LS 5039	4333.6782	0.986	−12.7	1.2	...
LS 5039	4333.7202	0.997	−11.2	0.5	...
LS 5039	4334.6263	0.229	23.0	3.2	...
LS 5039	4334.6788	0.242	29.1	9.2	...
LS 5039	4334.7103	0.250	34.6	14.8	...
LS 5039	4338.5552	0.234	22.5	2.7	...
LS 5039	4338.5973	0.245	18.2	−1.6	...
LS 5039	4338.6393	0.256	15.7	−4.1	...
LS 5039	4341.5908	0.011	−8.0	0.2	...
LS 5039	4341.6354	0.023	−11.9	−6.4	...
LS 5039	4341.6797	0.034	−4.2	−1.5	...
LS 5039	4342.5470	0.256	19.9	0.1	...
LS 5039	4342.5912	0.268	25.9	6.2	...
LS 5039	4342.6361	0.279	22.6	3.0	...
LS 5039	4343.5828	0.521	8.4	−1.5	...
LS 5039	4343.6293	0.533	9.6	0.3	...
LS 5039	4343.6734	0.545	8.2	−0.4	...
LS 5039	4346.5929	0.292	22.1	2.7	...
LS 5039	4346.6358	0.303	21.0	1.8	...
LS 5039	4346.6673	0.311	13.0	−5.9	...
LS 5039	4354.5347	0.325	13.1	−5.5	...
LS 5039	4354.5767	0.336	9.4	−8.9	...
LS 5039	4354.6187	0.347	20.9	3.0	...
LS 5039	4355.5278	0.580	−6.1	−12.6	...
LS 5039	4355.5705	0.590	−11.0	−16.7	...
LS 5039	4355.6133	0.601	−14.6	−19.6	...
LS 5039	4357.5744	0.103	−1.5	−13.2	...
LS 5039	4357.6174	0.114	11.9	−1.4	...
LS 5039	4357.5314	0.092	−0.2	−10.2	...
LS 5039	4358.6397	0.376	21.2	4.3	...
LS 5039	4358.5687	0.358	9.5	−8.0	...
LS 5039	4358.5263	0.347	5.5	−12.4	...
LS 5039	4360.5797	0.873	−27.5	−9.9	...
LS 5039	4360.5373	0.862	−27.0	−10.2	...
LS 5039	4360.6222	0.884	−21.1	−2.7	...
LS 5039	4525.8807	0.192	−2.6	−21.7	...

TABLE 1—*Continued*

Star	HJD (−2,450,000)	Orbital Phase	V_r (km s ^{−1})	($O - C$) (km s ^{−1})	ΔV_{ISM} (km s ^{−1})
LS 5039	4536.8753	0.006	−12.2	−2.7	...
LS 5039	4544.8626	0.051	−10.1	−11.6	...
LS 5039	4552.8287	0.091	11.8	2.1	...
LS 5039	4560.8249	0.138	15.8	−0.0	...
LS 5039	4569.7635	0.426	−8.2	−23.0	...

TABLE 2
ORBITAL ELEMENTS

	LS I +61 303	LS 5039
P (d)	26.4960 ^a	3.90608 ± .00010
T_0 (HJD−2,450,000)	1057.89 ± .23	2825.985 ± .053
e537 ± .034	.337 ± .036
ω (deg)	40.5 ± 5.7	236.0 ± 5.8
K_1 (km s ^{−1})	19.6 ± 1.1	19.74 ± .86
γ (km s ^{−1})	−41.41 ± .60	4.01 ± .31
$f(m)$ (M_\odot)	0.0124 ± .0022	.00261 ± .00036
$a_1 \sin i$ (R_\odot)	8.64 ± 0.52	1.435 ± 0.066
σ (km s ^{−1})	7.41	7.14

^aFixed.

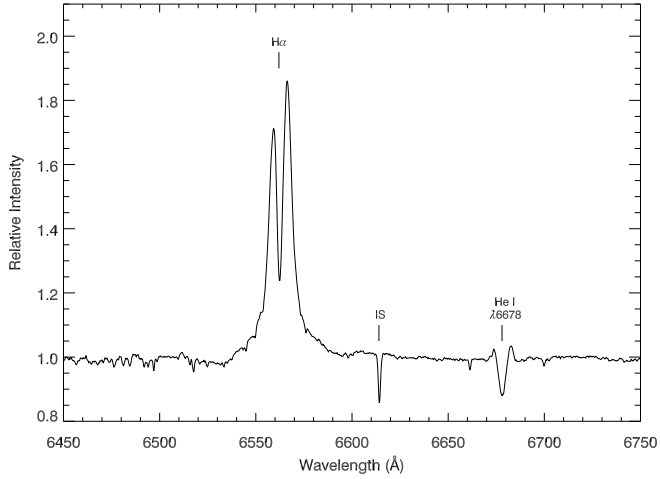


Fig. 1.— The final mean spectrum of LS I +61 303, formed by shifting each spectrum to its rest velocity to remove orbital variations. The red spectrum reveals strong emission in the H α line and weaker emission in the wings of the He I λ 6678 line.

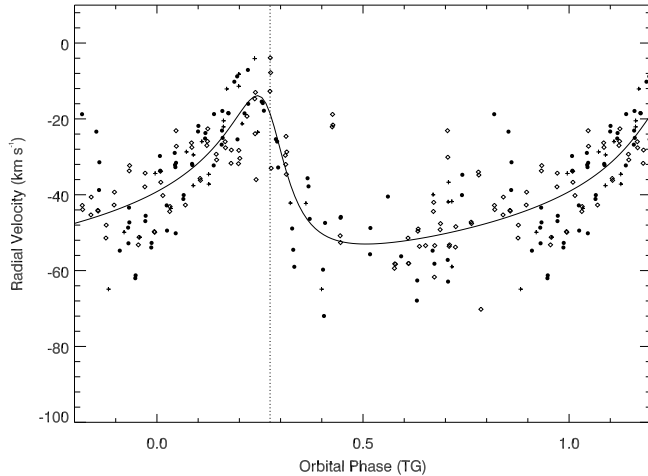


Fig. 2.— Radial velocity curve of LS I +61 303. Periastron corresponds to $\phi(\text{TG}) = 0.275$ and is marked as a dotted line in this plot. Points plotted as open diamonds are from Grundstrom et al. (2007a), crosses are from Casares et al. (2005a), and filled circles are from this work.

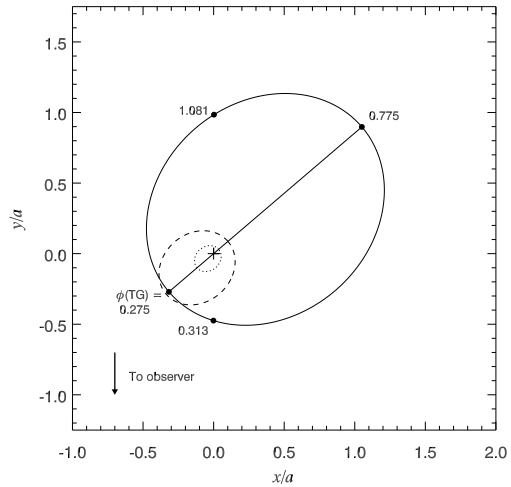


Fig. 3.— Orbital geometry of LS I +61 303, looking down on the orbital plane, showing the relative orbits (r/a) of the optical star ($12.5M_{\odot}$; Casares et al. 2005a) and its compact companion of unknown mass. The relative orbit of the compact object is shown as a solid line, while the Be star’s relative orbit depends greatly on the mass of the companion. The dashed line indicates the Be star’s orbit assuming a $4M_{\odot}$ black hole, while the dotted line assumes a $1.4M_{\odot}$ neutron star. The relevant phases of periastron, apastron, and conjunctions are marked along the orbit of the compact companion. The center of mass is indicated with a cross, and the thin solid line is the orbital major axis.

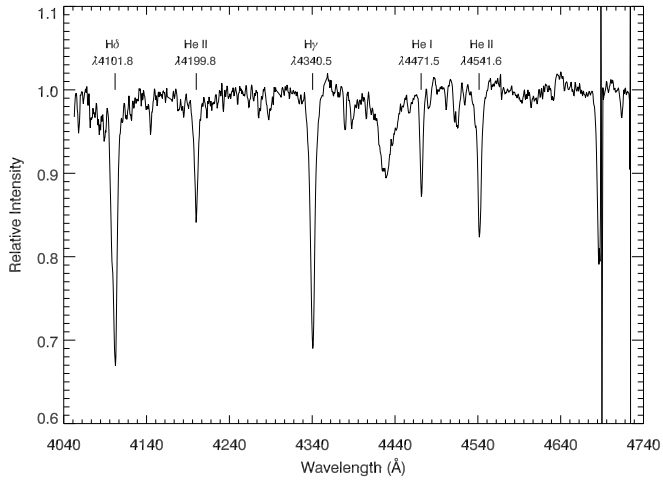


Fig. 4.— The mean spectrum of LS 5039 from the night of 2007 August 29, taken near the time of inferior conjunction of the optical star. We used this mean spectrum as a reference to determine the relative V_r by cross correlation with each spectrum of LS 5039.

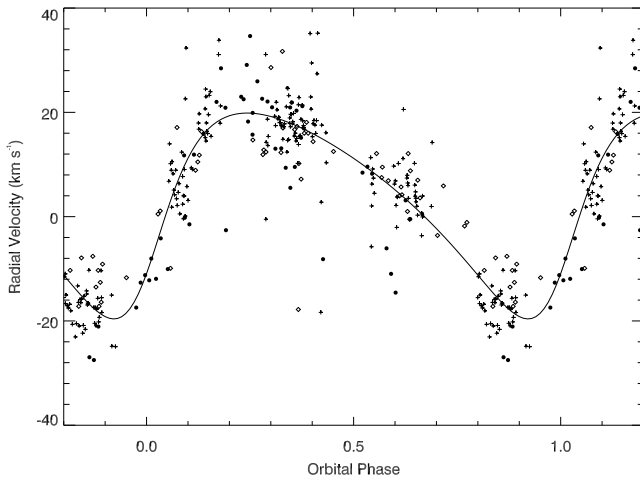


Fig. 5.— Radial velocity curve of LS 5039. Periastron corresponds to $\phi = 0$ in this plot. Points plotted as open diamonds are from McSwain et al. (2001, 2004), crosses are from Casares et al. (2005b), and filled circles are from this work.

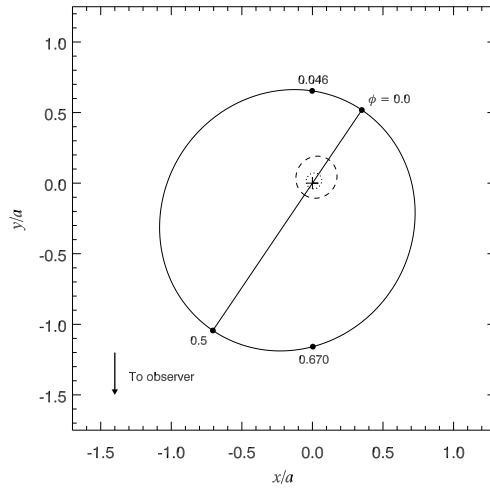


Fig. 6.— Orbital geometry of LS 5039, looking down upon the orbital plane, in a similar format to Fig. 3. Here, the optical star ($23M_{\odot}$; Casares et al. 2005b) orbits either a $3.7M_{\odot}$ black hole (Casares et al. 2005b) or a $1.4M_{\odot}$ neutron star.

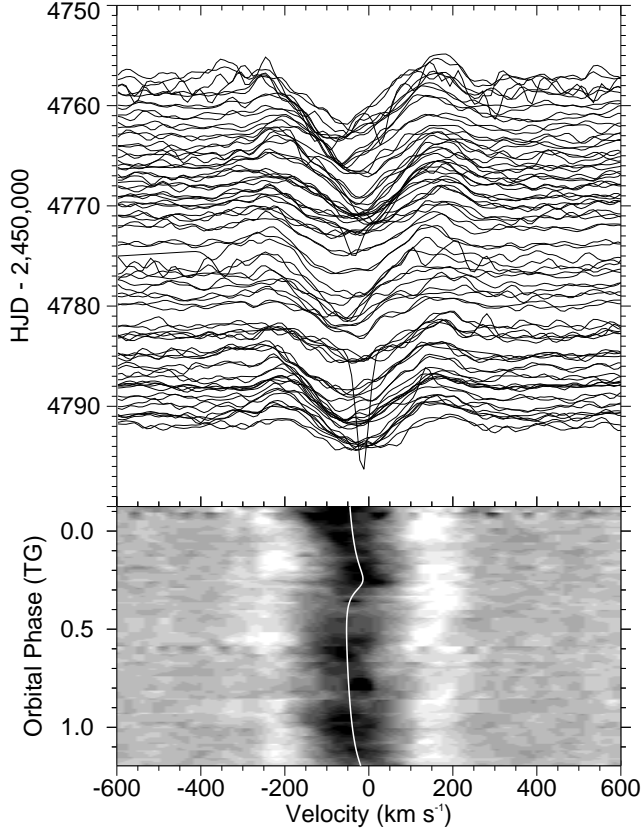


Fig. 7.— The upper plot shows the He I $\lambda 6678$ line profile of LS I +61 303 over our continuous 35 nights of observation, sorted by HJD and smoothed for clarity, and the lower plot shows a gray-scale image of the same line. Note that the lower plot of the gray-scale spectra are *not* folded by orbital phase but are placed in the same chronological order as the upper plot, with the orbital phases indicated. The intensity at each velocity in the gray-scale image is assigned one of 16 gray levels based on its value between the minimum (dark) and maximum (bright) observed values. The intensity between observed spectra is calculated by a linear interpolation between the closest observed phases. The solid white line shows the theoretical V_r curve solution.